Boise State University
ScholarWorks

Electrical and Computer Engineering Faculty Publications and Presentations

Department of Electrical and Computer Engineering

10-1-2009

Evolution of Chemical Structure During Silver Photodiffusion into Chalcogenide Glass Thin Films

A. Kovalskiy
Lehigh University

H. Jain
Lehigh University

Maria Mitkova
Boise State University

This is an author-produced, peer-reviewed version of this article. The final, definitive version of this document can be found online at *Journal of Non-Crystalline Solids*, published by Elsevier. Copyright restrictions may apply. DOI: 10.1016/j.jnoncrysol.2008.12.021

This is an author-produced, peer-reviewed version of this article. The final, definitive version of this document can be found online at Journal of Non-Crystalline Solids, published by Elsevier. Copyright restrictions may apply.
doi: 10.1016/j.jnoncrysol.2008.12.021

Evolution of chemical structure during silver photodiffusion into chalcogenide glass thin films

A. Kovalskiy[1], H. Jain[1], M. Mitkova[2]
[1]*Department of Materials Science, Lehigh University,*
5 East Packer Avenue, Bethlehem, PA 18015-3195, USA
e-mail: h.jain@lehigh.edu
[2]*Department of Electrical and Computer Engineering,*
Boise State University, 1910 University Dr., Boise, ID 83725-2075, USA

Abstract
The change of chemical structure resulting after X–ray and photo-induced silver diffusion into chalcogenide glass (ChG) thin films is monitored by high resolution X-ray photoelectron spectroscopy (XPS). $As_{40}S_{60}$ and $Ge_{30}Se_{70}$ thin films, which are based on pyramids and tetrahedral structural units, are investigated as model materials. Survey, core level (As 3*d*, S 2*p*, Ge 3*d*, Ge 2*p*, Se 3*d*, Ag $3d_{5/2}$, O 1*s*, C *1*s) and valence band spectra have been recorded and analyzed. Reference point for the binding energy is established by the subsequent deposition of thin gold film on top of the measured samples. The chemical structure gradually changes during diffusion of silver in all the samples. The mechanism of change depends on the chemical composition, thickness of the diffused silver layer and conditions of irradiation. It is revealed that surface oxygen can play important role in the Ag photodiffusion process, leading to phase separation on the surface of the films. Photodiffusion of Ag into $As_{40}S_{60}$ film leads to the formation of a uniform ternary phase and arsenic oxides on the surface. The formation of ethane-like $Ge_2(S_{1/2})_6$ units together with germanium oxidation are the main outcomes of X-ray induced Ag diffusion into $Ge_{30}Se_{70}$ film.

PACS codes: 71.23.Cq, 61.43.Fs, 66.30-hh

1. Introduction

The unique phenomenon of photoinduced Ag diffusion into ChG thin films is successfully exploited in photolithography and memory devices [1,2]. The mechanism of this effect has been studied by different experimental and theoretical methods [4-8], but atomistic and chemical origin of the observed structural transformations is still under discussion. High resolution X-ray photoelectron spectroscopy (XPS) is one of the most effective methods to examine the changes in chemical composition and electronic structure of the materials, which can be utilized also for photodiffusion studies. In our previous work [9,10], we investigated the mechanism of Ag photodiffusion into arsenic and germanium-based films that were thermally deposited within the vacuum of XPS spectrometer. Thus those samples never came in contact with air, and any potential interference of oxygen in the photodiffusion process was expressly avoided; the results focused simply on the well-defined interaction of Ag with glass matrix. In present work we extend the understanding of Ag photodiffusion under the conditions to be found in actual applications. Accordingly, the samples are prepared in two stages, and Ag is deposited on ChG films that are exposed to air beforehand.

It was shown earlier [11] that not only band gap light but also X-rays can cause photodiffusion. Therefore, our aim is also to assess X-ray vis-à-vis light-induced diffusion by high-resolution XPS, the former arising from the XPS experiment itself. The photo-induced changes in the electronic structure are determined for

This is an author-produced, peer-reviewed version of this article. The final, definitive version of this document can be found online at Journal of Non-Crystalline Solids, published by Elsevier. Copyright restrictions may apply.
doi: 10.1016/j.jnoncrysol.2008.12.021

both arsenic and germanium based chalcogenide glasses, with a focus on understanding the role of surface oxygen. One additional outcome of this study is that it gives idea about the products forming on the interface ChG–Ag which is a question of extended discussions.

2. Experimental procedures

The $As_{40}S_{60}$ and $Ge_{30}Se_{70}$ compositions have been chosen for this investigation of Ag photodiffusion. They represent two different types of chalcogenide glasses, which are built up by pyramidal and tetrahedral structural units, respectively. The stoichiometric arsenic sulfide is one of the most promising candidate materials for electron- and photo-lithography [12,13]. The selenium-rich germanium selenide is the material of choice for programmable metallization cells [2]. Both applications depend on Ag photodiffusion. So, amorphous Ag/$As_{40}S_{60}$ and Ag/$Ge_{30}Se_{70}$ bilayer thin film samples were prepared by thermal evaporation under $2{\cdot}10^{-6}$ Torr vacuum using Edwards E306A coating system. Chalcogenide glass films (thickness 200 nm for $Ge_{30}Se_{70}$ and 1 µm for $As_{40}S_{60}$) were deposited on HF-etched Si wafers (Wacker Siltronic Corp., 525 ± 20 µm thickness) from the bulk glass. In addition, 400 nm films from $Ge_{40}Se_{60}$ were prepared for structural evaluation. The thickness of silver layers evaporated on top of chalcogenide films was 40 nm for $As_{40}S_{60}$, 1.5 nm and 11.5 nm for $Ge_{30}Se_{70}$. Freshly prepared chalcogenide films were exposed to air for ~15 minutes before the XPS study.

The Ag/$As_{40}S_{60}$ samples were irradiated for 10 min in air with visible light from a halogen lamp (~15 mW/cm^2) through a IR cut off filter. For the Ag/$Ge_{30}Se_{70}$ bilayer structures the X-ray photons served simultaneously as XPS probe and as radiation driving the Ag photodiffusion.

The XPS spectra (core levels and valence band) were recorded by a Scienta ESCA-300 spectrometer with monochromatic Al K_α X-ray (1486.6 eV). The instrument was operated in a mode that yielded a Fermi-level width of 0.4 eV for Ag metal and a full width at half maximum (FWHM) of 0.54 eV for Ag $3p_{5/2}$ core level peak. Energy scale was calibrated using the Fermi level of pure Ag. The surface charging from photoelectron emission was controlled by flooding the surface with low energy (< 10 eV) electrons. The raw data were calibrated with a gold thin film using its $4f_{7/2}$ line position at 84.0 eV.

Data analysis was conducted with standard CASA-XPS software package. For analyzing the core-level spectra, Shirley background was subtracted and a Voigt line-shape, which results from a superposition of independent Lorentzian and Gaussian line broadening mechanisms, was assumed for the peaks [14]. Each 3*d* core-level spectrum for As, Ge and Se consisted of one or more spin orbit doublets splitting into $d_{5/2}$ and $d_{3/2}$ components. The 2*p* core level spectra of S contained spin orbit splitting doublets of $p_{3/2}$ and $p_{1/2}$ components. The experimental error in the peak position and area of each component was ±0.05 eV and ±2 %, respectively. More detailed description of fitting procedure can be found elsewhere [15].

3. Results

3.1. Ag/$As_{40}S_{60}$ bilayer

The fitting and analysis of As 3*d* and S 2*p* core level spectra for freshly prepared $As_{40}S_{60}$ film, which was exposed to air before XPS measurements, reveals two distinct chemical environments for sulfur and three components for arsenic. Each component consists of two peaks due to spin-orbit splitting of the *d* and *p* core levels (Fig 1). The estimated chemical composition of the film, as obtained from the areas of core level peaks, is $As_{41}S_{59}$. Irradiation of the freshly prepared layer by X-rays does not show any appreciable change either in the chemical composition or the structure of the core levels. We did not observe also any significant changes of XPS spectra after irradiation of the freshly deposited film by visible light (Table 1). The detailed parameters of fitting are presented in Table 1. In the first raw of the same Table, for comparison we include the data for $As_{40}S_{60}$ film deposited within the XPS chamber (i.e. never exposed to the ambient until after the experiment). The As $3d_{5/2}$ major peak (75 % of all As atoms) appears at 42.5 eV, and that of S $2p_{3/2}$ (78 % of S atoms) at 161.7 eV. These positions slightly differ from the binding energies published in some of our previous papers where gold reference was not used [9,13]. Here, we have made corrections using more reliable and precise referencing to Au $4f_{7/2}$ (at 84.0 eV).

This is an author-produced, peer-reviewed version of this article. The final, definitive version of this document can be found online at Journal of Non-Crystalline Solids, published by Elsevier. Copyright restrictions may apply.
doi: 10.1016/j.jnoncrysol.2008.12.021

We discover that the surface of the freshly prepared $As_{40}S_{60}$ film, which contacted with air, contained large amount of oxygen, most likely as OH complexes. For the non-irradiated film (sample 2, Table 1) the oxygen content was ~37.7 at. % (data are given in parenthesis in Table 1, when oxygen is not included in the calculated total composition of the sample surface); for irradiated sample (sample 3, Table 1) the O concentration decreases to 13.4 at. %. We did not notice considerable shift of O 1*s* binding energy between the two cases.

Two sets of XPS results were measured for Ag/$As_{40}S_{60}$ bilayer (samples 4 and 5, Table 1). The data for sample 4, taken just after Ag deposition, show that despite 40 nm top layer of Ag we were able to record not only Ag $3d_{5/2}$ but also As 3*d* and S 2*p* spectra. This is an indication that the Ag film is thinner than the penetration depth of the method, i.e. part of Ag has diffused into the As_2S_3 film under the influence of the X-rays of XPS spectrometer. However, based on our previous experience [9], under the conditions used here, X-ray exposure is not expected to affect the structure of $As_{40}S_{60}$ films or Ag/$As_{40}S_{60}$ bilayers that have been already exposed to visible light. The structure of As 3*d* peak for Ag/$As_{40}S_{60}$ bilayer differs from the one for $As_{40}S_{60}$ as it contains two As $3d_{5/2}$ components: one at 41.9 eV which is the same as for $As_{40}S_{60}$ without Ag, and a new component at 43.8 eV. The S 2*p* peak is considerably shifted to the lower binding energies in comparison with that for $As_{40}S_{60}$. S $2p_{3/2}$ also has two components at 160.5 (70 % of all S atoms) and 161.1 eV. S/As ratio for the sample is the same as in the case of $As_{40}S_{60}$ film without any silver. Oxygen concentration is ~ 45.2 at. %. The binding energy of Ag $3d_{5/2}$ peak at 367.5 eV significantly differs from the position for metallic Ag (368.3 eV [16]). Calculated concentration of Ag on the analyzed surface of sample 4 (Table 1) is 20.7 at. %
.
The second set of data was collected after 10 min of irradiation with visible light. The component at higher binding energies (43.8 eV – 40 % of all As atoms) persists, however, two new components appear at lower energies (at 41.4 eV (57 at. %) and 40.1 eV (3 at. %)). The chemical environment of S atoms becomes uniform after exposure to light with only one S $2p_{3/2}$ component at 160.7 eV. There is a decrease in oxygen concentration from 45.2 to 39.3 at. %, which is accompanied by large chemical shift (~ 1.3 eV) to higher binding energies. Silver concentration on the surface decreases from 20.7 to 10.0 at. % due to illumination.

3.2. Ag/$Ge_{30}Se_{70}$ bilayer

Both Ge 3*d* and Se 3*d* core level spectra of the surface of freshly deposited $Ge_{30}Se_{70}$ thin film exhibit two doublet components (30.8 eV and 30.2 eV for Ge $3d_{5/2}$; 54.3 eV and 54.8 eV for Se $3d_{5/2}$). They are similar to the spectra registered for the films evaporated inside the UHV chamber of XPS spectrometer (Table 2). In contrast to $As_{40}S_{60}$ film, we observe very low concentration of oxygen on the surface even after the sample is exposed to air, although the position (531.7 eV) is the same for O 1*s* peaks. The Ge/Se ratio of the deposited film matches well with that of the bulk glass used for evaporation.

The chemical structure of the surface region of Ag/$Ge_{30}Se_{70}$ bilayer depends on the thickness of Ag film deposited on top of $Ge_{30}Se_{70}$ film. The position of Ge 3*d* and Se 3*d* and O 1*s* core level peaks shifts gradually to lower binding energies with increasing Ag layer thickness (Fig. 2, Table 2). Simultaneously, we observe a new minor component of Ge 3*d* core level on the higher binding energy side (Table 2). The surface concentration of oxygen increases with every new deposition, in proportion to the time of exposure to air. The maximum concentration of silver on the surface was found to be around 15.6 at. % for the Ag film of 115 Å thickness deposited on 200 nm $Ge_{30}Se_{70}$ film. Spectral position of Ag $3d_{5/2}$ peak differs from the usual location of metal Ag component by around 1 eV.

3.3. $Ge_{40}Se_{60}$ thin films

To obtain XPS reference data for Ge-rich glasses, $Ge_{40}Se_{60}$ thin film, consisting mostly of ethane-like $Ge_2(Se_{1/2})_6$ units [17], was examined. Before the XPS measurements this film was exposed to air for a short time (~ 15 min) needed to transfer the sample from the thermal evaporator to XPS spectrometer chamber. The major Ge $3d_{5/2}$ and Se $3d_{5/2}$ components of the core levels are found at 30.2 and 54.3 eV, respectively (Fig. 3). The Ge 3*d* core level contains also two minor components at higher binding energies.

This is an author-produced, peer-reviewed version of this article. The final, definitive version of this document can be found online at Journal of Non-Crystalline Solids, published by Elsevier. Copyright restrictions may apply.
doi: 10.1016/j.jnoncrysol.2008.12.021

4. Discussion

XPS is a surface analysis technique with about 65% of the signal originating from the outermost ~30 Å of the film [18]. Consequently, two important comments should be made before we start analyzing the present experimental results. First of all, the observed changes of electronic structure on the surface do not necessarily correspond to the chemical transformation deep inside the films. Secondly, the satisfactory level of the XPS signal for As, S, Ge, Se core level peaks from the underlying chalcogenide layers is the first confirmation of silver diffusion inside the film body.

XPS data analysis is based on the dependence of binding energy for the studied core levels on the oxidation state of various chemical elements. For covalently bonded solids the position (or binding energy) of a core level XPS peak of a given atom would shift with respect to normal position as a result of changes in its coordination or charge density, and substitution of one or more of its neighbors by a chemical element with different electronegativity or charge state. That is, any change in the chemical environment of an atom would be directly reflected in its core level binding energies.

Next we discuss the results described in the previous section for three glass compositions. Due to space limitation, selected XPS spectra are shown, but the two Tables contain relevant parameters for all the investigated conditions.

4.1 Photodiffusion in $Ag/As_{40}S_{60}$ bilayer

Core level spectra of freshly deposited $As_{40}S_{60}$ film (Fig. 1, Table 1) confirm the existence of several types of structural fragments. The major component of As 3*d* spectrum at 42.5 eV[1] corresponds to the regular pyramidal AsS_3 units, while the 41.9 eV component is from the occurrence of dispersed As-As "wrong" homopolar bonds. The third and the weakest component at 43.1 eV is of essentially surface origin representing As-O like bonds. However, it is not due to rather ionic As-O bonds in As_xO_y oxide, because its binding energy is not sufficiently high. Most probably, it represents an As-O bond formed by the replacement of one of the As-S bonds in AsS_3 pyramid. These pyramids, as in the case of $As_{40}S_{60}$ bulk glass, are mostly linked through As-S-As fragments (represented by the S $2p_{3/2}$ peak at 161.7 eV in S 2*p* spectrum). The doublet associated with 2-fold coordinated sulfur within As-S-S fragments should be situated at a higher binding energy within the S 2*p* spectrum due to the higher electronegativity of S atoms in comparison to As atoms.

Irradiation of freshly deposited $As_{40}S_{60}$ film with visible light does not decrease the concentration of homopolar bonds. However, this observation disagrees with the decrease of homopolar bond concentration observed after illumination of freshly deposited film by vibrational spectroscopy methods [19]. We believe this discrepancy is due to the surface limitation of the XPS technique vs. other optical spectroscopies.

Substantial decrease of oxygen concentration after light irradiation suggests 'photoannealing' or 'photo-removal' of OH-based fragments. We observed recently the same phenomenon when investigating photoinduced effects in ChG using synchrotron radiation for XPS studies. Interestingly, there is no noteworthy formation of As_2O_3 from the oxidation of $As_{40}S_{60}$ films under these conditions of irradiation, which should have shifted O 1*s* peak by ~ 1.0 eV [20], rather than the observed shift of only 0.4 eV).

XPS spectra of the $Ag/As_{40}S_{60}$ bilayer registered just after Ag deposition give us information on the structural transformations during the initial stage of silver diffusion (Fig. 4, Table 1). There is no more As $3d_{5/2}$ component at 42.5 eV associated with AsS_3 pyramids. Instead we observe two components of similar intensity, one of which at 43.8 eV (48 % of all As atoms) is attributed to arsenic oxide (As_2O_3), and the other at 41. 9 eV (52 % of all As atoms) is linked to the As bonded with 1As and 2S atoms (Table 1). The same fragments at 41.9 eV with concentration 11 at. % are present also in freshly deposited $As_{40}S_{60}$ film. The formation of arsenic oxide in silver photodiffused sample is supported by the shift of O 1*s* core level position to lower binding energies [20]. The S 2*p* spectrum of this sample reveals that there are no chemical

[1] All the binding energies are referred to the larger component of a given doublet e.g. for As $3d_{5/2}$ rather than As $3d_{3/2}$)

This is an author-produced, peer-reviewed version of this article. The final, definitive version of this document can be found online at Journal of Non-Crystalline Solids, published by Elsevier. Copyright restrictions may apply.
doi: 10.1016/j.jnoncrysol.2008.12.021

states of S atoms which existed in freshly deposited arsenic sulfide. Silver actively reacts with sulfur producing two new environments for S atoms. The detailed analysis supports the idea that one of the component at 161.1 eV (30 at. %) relates to the S within some kind of As-S-Ag fragments resulting from the break up of AsS_3 pyramids. The other component at 160.5 eV (70 at. %) clearly belongs to a more ionic ternary phase.

Irradiation of the $Ag/As_{40}S_{60}$ sample with visible light produces even larger changes in the chemical structure (Figs. 4 and 5, Table 1). Only one chemical state is found for S atoms in this case. Most probably, the light helped to dissolve separated As-S-Ag fragments in the above mentioned ternary phase, stabilizing the latter. This conclusion is consistent with the decreasing FWHM value of the ternary phase component from 1.3 to 0.9 eV. The chemical composition of the ternary phase can not be established, because Ag concentration is still far from its saturation, but S/As ratio in this phase is established to be close to 3. Apparently, we are observing an underdeveloped Ag_3AsS_3 phase [21]. The As 3*d* core level spectrum of light irradiated $Ag/As_{40}S_{60}$ consists of two distinct components: As in As_2O_3 (43.8 eV, 40 % of As atoms) and As within the ternary phase (160.7 eV, 57 % of As atoms). Existence of Ag-containing compound follows also from the chemical shift of Ag $3d_{5/2}$ position by ~1.0 eV towards lower binding energies in comparison with metallic Ag. Finally, some traces of light-induced As clustering (~3 at. % of all As atoms) can also be observed.

4.2. Photodiffusion in $Ag/Ge_{30}Se_{70}$ bilayer

In the Se-rich freshly deposited $Ge_{30}Se_{70}$ thin film the major peaks at 30.8 eV (Ge $3d_{5/2}$) and 54.3 eV (Se $3d_{5/2}$) correspond to tetrahedral $GeSe_4$ and Ge-Se-Ge fragments, respectively. Minor components at 30.2 eV and 54.8 eV relate to structural fragments with "wrong" homopolar bonds. Se-rich compositions do not oxidize from exposure to air. However, Ge-rich films, like $Ge_{40}Se_{60}$ (Fig. 3a) immediately oxidize even without light exposure. This could be one of the main reasons why Se-rich $Ge_{30}Se_{70}$ is considered as more appropriate medium for silver diffusion than Ge-rich films.

Deposition of very thin film of a few Ag monolayers (15 Å) on top of the $Ge_{30}Se_{70}$ film leads to a slight shift (~ 0.3 eV) of the major Ge 3*d* component to lower energies, presumably due to the addition of silver that has lower electronegativity than the matrix. From Ge 3*d* spectrum we observe also the formation of $Ge_2(S_{1/2})_6$ ethane-like units (30.0 eV, 11 % of Ge atoms). Their presence is confirmed by comparing with the spectra of $Ge_{40}Se_{60}$ films that are predominantly build up by such units (Fig. 3). Confirmation about formation of ethane like units after Ag diffusion in this glass has been established also by Raman spectroscopy [2]. During X-ray-induced Ag diffusion, we find traces of germanium oxidation (31.9 eV, ~2 at. % of Ge atoms) manifested by the O 1s peak slight shift (~0.3 eV) towards lower binding energy position. Some of the Se atoms (59 at. %) still preserve the major chemical environment of pure $Ge_{30}Se_{70}$ thin film in the form of Ge-Se-Ge fragments. However, the remaining Se atoms (41 at. %) experience the neighborhood of Ag atoms, shifting the position of Se $3d_{5/2}$ component to 53.6 eV. Position of Ag $3d_{5/2}$ component at 367.6 eV testifies that Ag is in a non-metallic chemically bonded state in the matrix.

Additional deposition of 100 Å layer of Ag enhances the observed changes in the chemical structure of $Ag/Ge_{30}Se_{70}$ bilayer. The ethane-like units become dominant in the structure (91 % of Ge atoms). The rest of Ge is attributed to germanium oxidation during silver diffusion (surface Ge-O bonds attached to ChG network reveal at 31.6 eV, germanium oxide – at 32.6 eV) causing the further shift of O 1*s* peak towards lower binding energies (531.1 eV). The analysis of Se 3*d* core level spectrum shows that most of Se (81 at.%) is within Ge-Se-Ag fragments, where Ag atoms are in between of Se atoms from different ethane-like units. We cannot confirm ionic or covalent character of Se-Ag bond, concluding only that the Ag atoms are in non-metallic bonds. There are also convincing data from XRD studies showing formation of Ag_2Se and Ag_8GeSe_6 after Ag diffusion in $Ge_{30}Se_{70}$ films [22] and we believe that the results in the studied case evident the initial stages of formation of these diffusion products. The remaining 19 at. % Se atoms reveal themselves at 53.9 eV, representing bridging atoms between two ethane-like units.

This is an author-produced, peer-reviewed version of this article. The final, definitive version of this document can be found online at Journal of Non-Crystalline Solids, published by Elsevier. Copyright restrictions may apply.
doi: 10.1016/j.jnoncrysol.2008.12.021

The above discussion shows not only possible mechanism of Ag diffusion into ChG films but reveals also that surface oxygen plays an important role in the Ag photodiffusion process, leading to phase separation on the surface of the films. As a result, the photodiffusion products on the surface will differ from those in the bulk. The surface phase separation may complicate the practical application of Ag photodiffusion, such as in grayscale reactive ion etching or a lithography process for making high resolution patterns [1].

5. Conclusions

High resolution XPS measurements of thermally deposited $As_{40}S_{60}$ and $Ge_{30}Se_{70}$ thin films reveal the presence of chemical states associated with pyramidal AsS_3 and tetrahedral $GeSe_4$ structural units, respectively, as well as "wrong" homopolar bonds. In the presence of oxygen photodiffusion of silver into $As_{40}S_{60}$ thin film leads to the formation of two-phase surface structure, consisting of arsenic oxide and an Ag-As-S ternary phase. It may limit the resolution of patterns formed by dry/wet etching based on Ag photodiffusion. In the case of X-ray induced diffusion of Ag into Ge-rich $Ge_{30}Se_{70}$, the surface consists of linked and broken ethane-like $Ge_2(S_{1/2})_6$ units and minor phase formed by germanium oxidation. The oxidation leads to structural differences between the surface and bulk of ChG films, which may be a limitation for certain practical applications of the photodiffusion effect. The new data obtained using Au $4f_{7/2}$ (84.0 eV) reference could serve as a reference for further studies of ChG electronic structure.

Acknowledgements

Separate parts of this work were supported by a Lehigh University – Army Research Lab (ARL) collaborative research program, the Pennsylvania Department of Community and Economic Development through the Ben Franklin Technology Development Authority and the National Science Foundation through the International Materials Institute for New Functionality in Glass (IMI-NFG) (NSF Grant No. DMR-0409588).

References

[1] A. Kovalskiy, M. Vlcek, H. Jain, A. Fiserova, C. M. Waits, M. Dubey, J. Non-Cryst. Solids 352 (2006) 589.

[2] M. Mitkova, M. N. Kozicki, J. Non-Cryst. Solids 299-302 (2002) 1023.

[3] T. Wagner, A. Mackova, V. Perina, E. Rauhala, A. Seppala, S. O. Kasap, M. Frumar, Mir. Vlcek, Mil. Vlcek, J. Non-Cryst. Solids 353 (2002) 1028.

[4] G. Kluge, Phys. Status Solidi A 101(1987) 105.

[5] De Nyago Tafen, D. A. Drabold, M. Mitkova, Phys. Rev. B 72 (2005) 054206
.

[6] A. V. Stronski, M. Vlcek, A. I. Stetsun, A. Sklenar, P. E. Shepeliavyi, J. Non-Cryst. Solids 270 (2000) 129.

[7] A. V. Kolobov, S. R. Elliott, Adv. Phys. 40 (1991) 625.

[8] A. Fischer-Colbrie, A. Bienenstock, P. H. Fuoss, M. A. Marcus, Phys. Rev. B 38 (1988) 12388.

[9] H. Jain, A. Kovalskiy, A. Miller, J. Non-Cryst. Solids 352 (2006) 562.

[10] A. Kovalskiy, A. C. Miller, H. Jain, M. Mitkova, J. Am. Ceram. Soc. 91 (2008) 760.

[11] K. D. Kolwicz, M. S. Chang, J. Electrochem. Soc. 127 (1980) 135.

[12] J. Neilson, A. Kovalskiy, M. Vlcek, H. Jain, F. Miller, J, Non-Cryst. Solids 353 (2007) 1427.

This is an author-produced, peer-reviewed version of this article. The final, definitive version of this document can be found online at Journal of Non-Crystalline Solids, published by Elsevier. Copyright restrictions may apply.
doi: 10.1016/j.jnoncrysol.2008.12.021

[13] A. Kovalskiy, H. Jain, J. Neilson, M. Vlcek, C. M. Waits, W. Churaman, M. Dubey, J. Phys. Chem. Solids 68 (2007) 920.

[14] J. M. Conny, C. J. Powell, Surf. Interface Anal. 29 (2000) 856.

[15] R. Golovchak, A. Kovalskiy, A.C. Miller, H. Jain, O. Shpotyuk, Phys. Rev. B 76 (2007) 125208.

[16] W. Huang, Z. Jiang, F. Dong, X. Bao, Surf. Sci. 514 (2002) 420.

[17] S. Mamedov, D.G. Georgiev, Tao Qu, P. Boolchand, J. Phys.: Condens. Mat. 15 (2003) S2397.

[18] D. Briggs, M.P. Seah (Eds.), Practical surface analysis, Vol. 1, 2nd ed., John Wiley & Sons Ltd., Chichester, New York, 1990, 483 p.

[19] O. I. Shpotyuk, Phys. Status Solidi B 183 (**1**994) 365.

[20] J. F. Moulder, W. F. Stickle, P. E. Sobol, K. D. Bomben, in: J. Chastein (Ed.), Handbook of X-ray Photoelectron Spectroscopy, Perkin-Elmer, Eden Prairie, MN, 1992.

[21] T. Kawaguchi, Jpn. J. Appl. Phys. 37 (1998) 29.

[22] M. Mitkova, M. N. Kozicki, J. Phys. Chem. Solids 68 (2007) 866.

Figure captions

Figure 1. X-ray photoelectron spectra of As 3*d* (*a*) and S 2*p* (*b*) core levels for freshly deposited and exposed to air $As_{40}S_{60}$ thin film.

Figure 2. Evolution of Ge 3*d* and Se 3*d* XPS core level spectra with deposition of Ag layer onto $Ge_{30}Se_{70}$ thin film preliminarily exposed to air.

Figure 3. X-ray photoelectron Ge 3*d* (*a*) and Se 3*d* (*b*) core level spectra of freshly deposited and exposed to air $Ge_{40}Se_{60}$ thin film.

Figure 4. XPS As 3*d* core level spectra of freshly deposited $As_{40}S_{60}$ thin film and Ag/$As_{40}S_{60}$ bilayer irradiated 10 min by halogen lamp (W=15 mW/cm2)

Figure 5. XPS Se 3*d* core level spectra of freshly deposited $As_{40}S_{60}$ thin film and Ag/$As_{40}S_{60}$ bilayer irradiated 10 min by halogen lamp (W=15 mW/cm2)

This is an author-produced, peer-reviewed version of this article. The final, definitive version of this document can be found online at Journal of Non-Crystalline Solids, published by Elsevier. Copyright restrictions may apply.
doi: 10.1016/j.jnoncrysol.2008.12.021

Tables

Table 1. Parameters of XPS analysis for Ag/$As_{40}S_{60}$ bilayer

Sample	Chemical composition					As 3*d* 5/2-I	As 3*d* 5/2-II	As 3*d* 5/2-III	S 2*p* 3/2-I	S 2*p* 3/2-II	S 2*p* 3/2-III	Ag 3*d* 5/2	O 1*s*
	S/As	As	S	Ag	O	eV at. % FWHM						eV	
		at. %											
Sample 1 $As_{40}S_{60}$ in UHV	1.58	38.8	61.2	-	-	41.9 7 0.67	42.5 93 0.67	-	-	161.6 86 0.78	162.3 14 0.68	-	-
Sample 2 $As_{40}S_{60}$ exposed to air	1.43	41.0	59.0	-	(37.7)	41.9 11 0.76	42.5 75 0.86	43.1 14 1.28	-	161.7 78 0.93	162.5 22 1.01	-	531.7
Sample 3 $As_{40}S_{60}$ exposed to air, irradiated	1.44	40.9	59.1	-	(13.4)	42.0 11 0.71	42.5 77 0.77	43.0 12 0.96	-	161.7 75 0.84	162.4 25 0.95	-	531.3
Sample 4 $As_{40}S_{60}$ exposed to air +40 nm Ag	1.41	32.9	46.4	20.7	(45.2)	41.9 52 1.19	-	43.8 48 1.38	160.5 70 0.81	161.1 30 1.30	-	367.5	529.5
Sample 5 $As_{40}S_{60}$ exposed to air +40 nm Ag+ irradiated	1.62	34.3	55.7	10.0	(39.3)	40.1 3 0.68	41.4 57 1.15	43.8 40 1.56	160.7 100 0.90	-	-	367.3	530.8
Pure Ag	-	-	-	100	-	-	-	-	-	-	-	368.3	-

Table 2. Parameters of XPS analysis for Ag/$Ge_{30}Se_{70}$ bilayer

Sample	Chemical composition					Ge 3*d* 5/2-I	Ge 3*d* 5/2-II	Ge 3*d* 5/2-III	Se 3*d* 3/2-I	Se 3*d* 3/2-II	Se 3*d* 3/2-III	Ag 3*d* 5/2	O 1*s*
	Se/Ge	Ge	Se	Ag	O	eV at. % FWHM						eV	
		at. %											
Sample 6 $Ge_{30}Se_{70}$ deposited at UHV [10]	2.46	28.9	71.1	-	-	30.7 88 0.71	30.3 12 0.86	-	54.7 17 0.78	54.2 83 0.82	-	-	-
Sample 7 $Ge_{30}Se_{70}$ exposed to air	2.42	29.2	70.8	-	(4.3)	30.8 96 0.81	30.2 4 0.73	-	54.8 12 0.73	54.3 88 0.87	-	-	531.7
Sample 8 $Ge_{30}Se_{70}$ exposed to air + 15 Å Ag	2.49	25.2	62.8	12.0	(8.1)	31.9 2 0.55	30.5 87 0.82	30.0 11 0.91	-	54.1 59 0.89	53.6 41 0.93	367.6	531.4
Sample 9 $Ge_{30}Se_{70}$ exposed to air + 115 Å Ag	2.34	25.3	59.1	15.6	(18.0)	32.6 2 0.93	31.6 7 0.97	30.1 91 0.99	-	53.9 19 0.79	53.4 81 1.02	367.4	531.1
Pure Ag	-	-	-	100	-	-	-	-	-	-	-	368.3	-

This is an author-produced, peer-reviewed version of this article. The final, definitive version of this document can be found online at Journal of Non-Crystalline Solids, published by Elsevier. Copyright restrictions may apply.
doi: 10.1016/j.jnoncrysol.2008.12.021

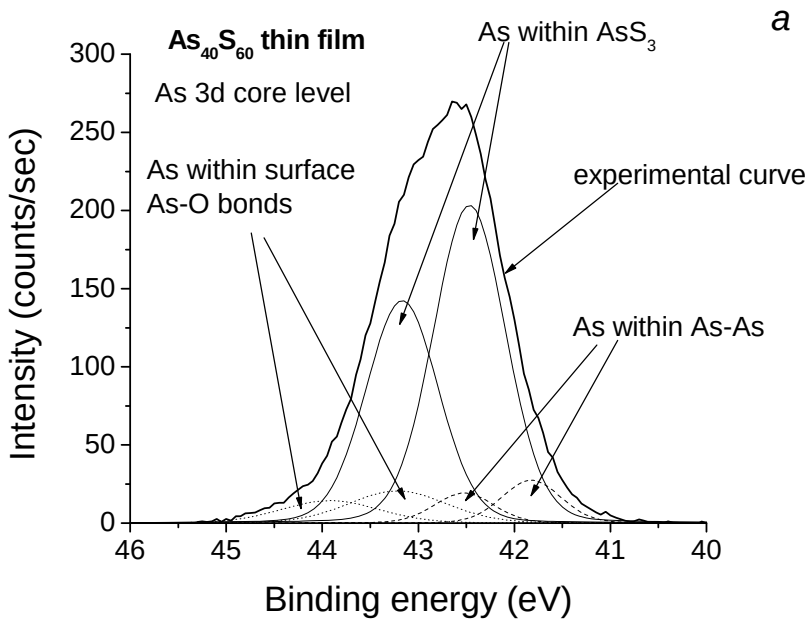

Fig. 1a

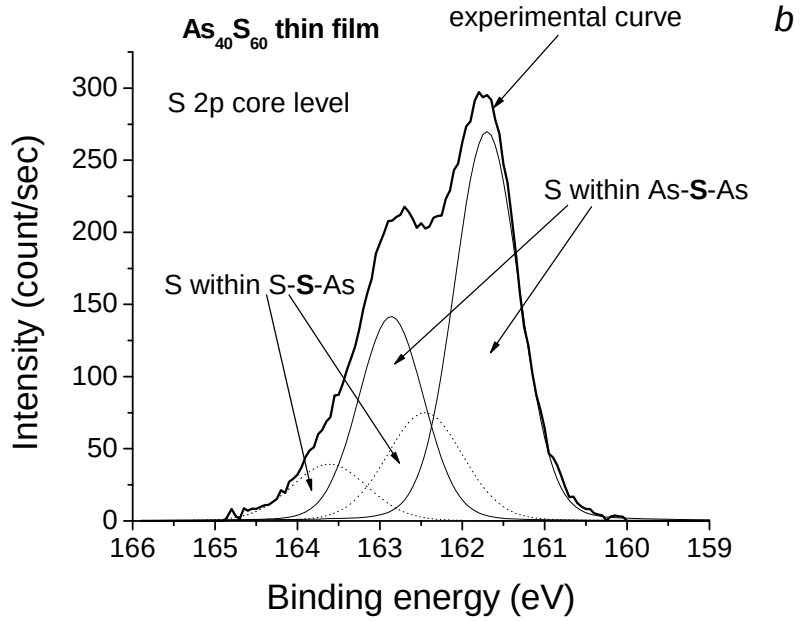

Fig. 1b

This is an author-produced, peer-reviewed version of this article. The final, definitive version of this document can be found online at Journal of Non-Crystalline Solids, published by Elsevier. Copyright restrictions may apply.
doi: 10.1016/j.jnoncrysol.2008.12.021

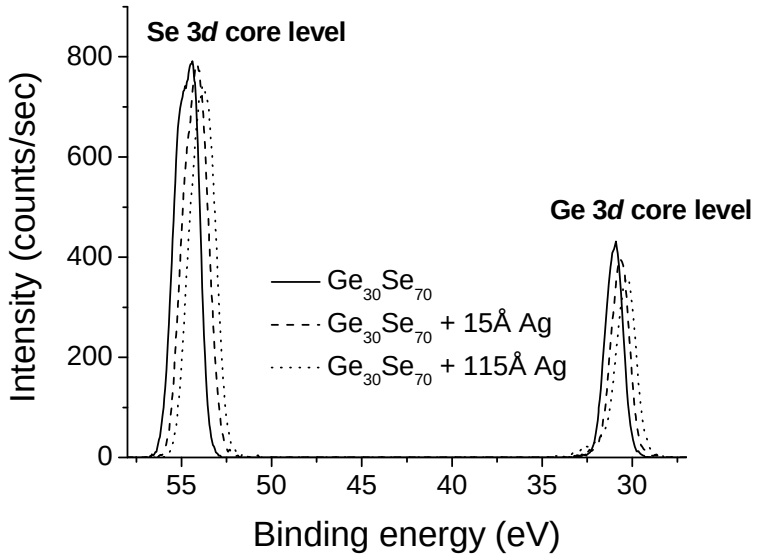

Fig. 2.

This is an author-produced, peer-reviewed version of this article. The final, definitive version of this document can be found online at Journal of Non-Crystalline Solids, published by Elsevier. Copyright restrictions may apply.
doi: 10.1016/j.jnoncrysol.2008.12.021

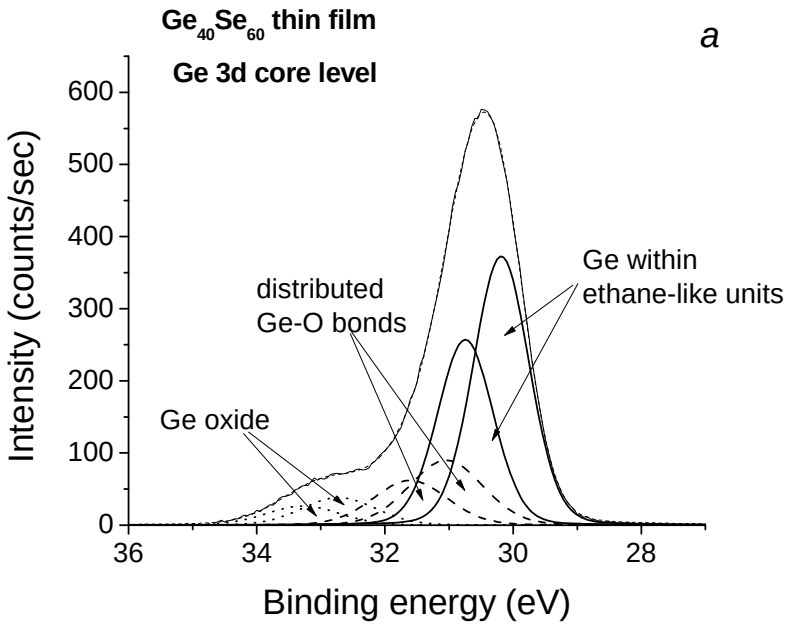

Fig. 3a

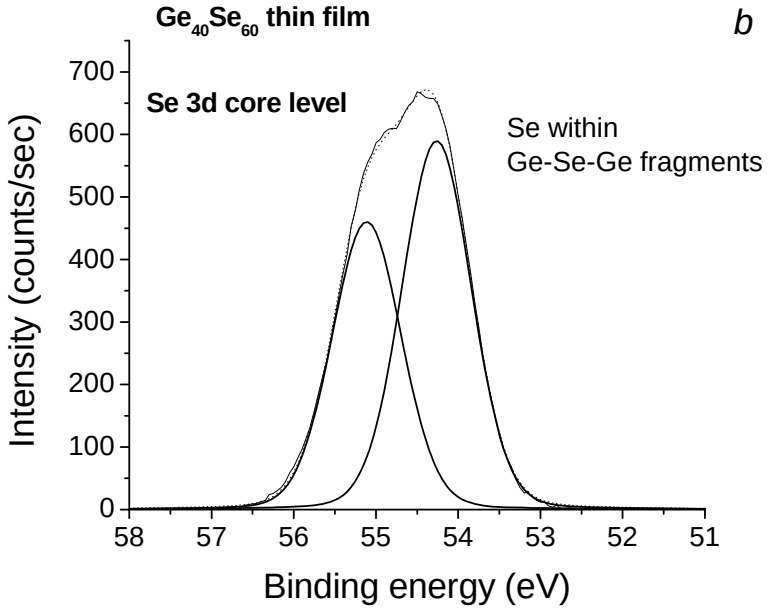

Fig. 3b

This is an author-produced, peer-reviewed version of this article. The final, definitive version of this document can be found online at Journal of Non-Crystalline Solids, published by Elsevier. Copyright restrictions may apply.
doi: 10.1016/j.jnoncrysol.2008.12.021

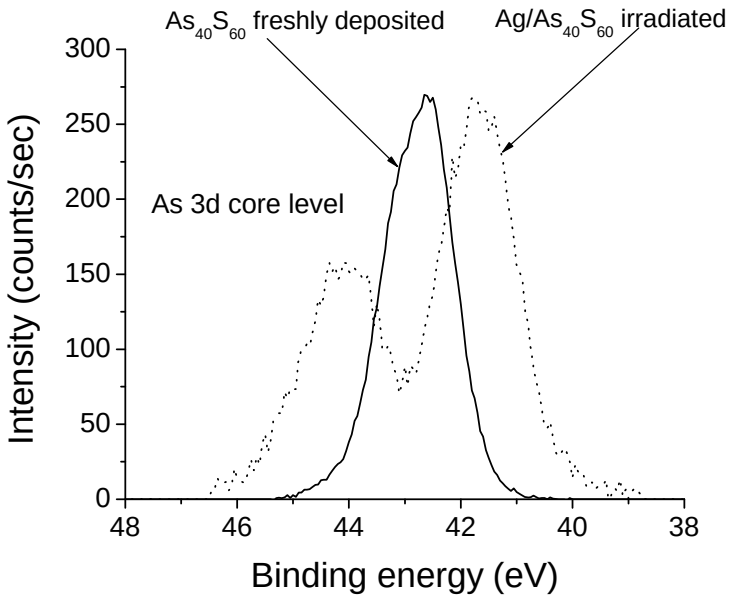

Fig. 4.

This is an author-produced, peer-reviewed version of this article. The final, definitive version of this document can be found online at Journal of Non-Crystalline Solids, published by Elsevier. Copyright restrictions may apply.
doi: 10.1016/j.jnoncrysol.2008.12.021

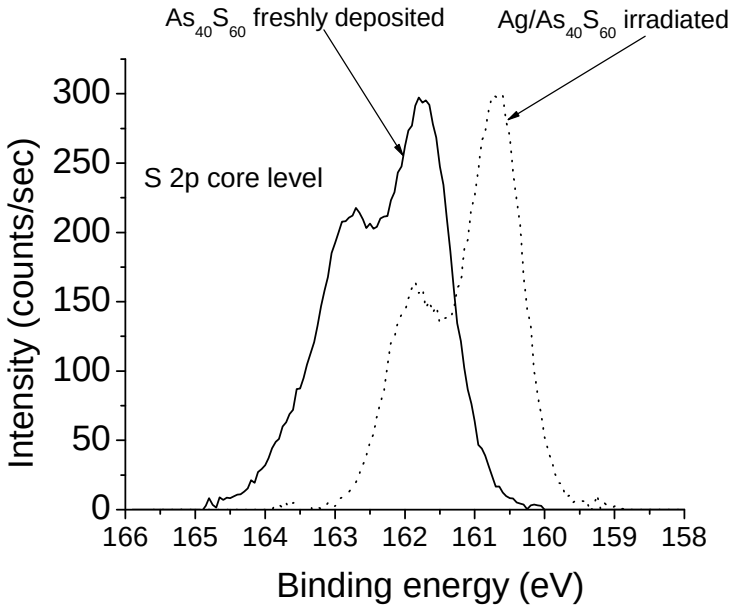

Fig. 5